

Development of a mouse computational model for MCNPx based on Digimouse[®] images and dosimetric assays

Bruno Melo Mendes^{1,2}, Iassudara Garcia de Almeida², Bruno Machado Trindade², Telma Cristina Ferreira Fonseca¹, Tarcísio Passos Ribeiro de Campos²

¹Centro de Desenvolvimento da Tecnologia Nuclear (CDTN/CNEN), Belo Horizonte, MG, Brasil, ²Departamento de Engenharia Nuclear, DEN, Programa de Pós-Graduação em Ciências e Técnicas Nucleares, Universidade Federal de Minas Gerais, UFMG, Belo Horizonte, MG, Brasil

The aim of this study was to create and test a new mice 3D-voxel phantom named DM_BRA for mice and human first-estimation radiopharmaceutical dosimetry. Previously, the article reviews the state-of-art in animal model development. Images from Digimouse CT database were used in the segmentation and on the generation of the voxelized phantom. Simulations for validation of the DM_BRA model was performed at 0.015, 0.1, 0.5, 1 and 4 MeV photons with heart-source. Specific Absorbed Fractions (SAF) data were compared with literature data. The organ masses of DM_BRA correlated well with existing models based on the same dataset; however, few small organ masses hold significant variations. The SAF data in most simulated cases were statistically equal to a significant level of 0.01 to the reference data.

Uniterms: Dosimetry/assay. Mouse phantom/tests. MCNPx Monte Carlo code Computational studies.

INTRODUCTION

Small animals, such as mice, have been widely used in experimental protocols involving ionizing radiation. Biodistribution studies have often been conducted in murine to obtain a first estimation of the absorbed doses in humans (Stabin *et al.*, 2006). The animal absorbed doses estimation, in most cases, do not reach values which can bias the experimental results (Carlson *et al.*, 2007). However, experimental methods have often included extensive image generation (MicroCT and/or PET/SPECT) and radiopharmaceuticals therapeutic doses administration that provide a large absorbed dose in the experimental animals. Previous work has shown that even low absorbed doses (50 to 500 mGy) can induce biological effects in mice (Wang, Cai, 2000; Yonezawa, 2006). In such cases, the accurate quantification of absorbed doses and the determination of the energy deposition patterns are of fundamental importance to qualify or exclude potential radiobiological effects that may interfere with in vivo experiments.

The physical measurement of absorbed doses can be performed by TLD or another kind of dosimeter (like MOSFET) implanted in interest organs or tissues (Stabin *et al.*, 2006; Carlson *et al.*, 2007; Kolbert *et al.*, 2003, Flynn *et al.*, 2001). However, the invasiveness of these procedures is the primary limiting factor for their use in preclinical and clinical practices.

An alternative approach that has been successful in dosimetric evaluations is the use of computational models coupled to radiation transport codes (Snyder, Ford, Warner, 1978; Petoussi-Henss, Zankl, 1998; Xu, Eckerman, 2009; ICRP, 2009). The pioneering mice computational models, namely mouse phantoms, emerged in the 90s. The work of Hui *et al.* (1994) is usually the first model referenced. This group created a stylized phantom based on geometric shapes described by simple mathematical equations. Yoriyaz, Stabin (1997) developed another analytical phantom adopting a 30 g mouse as a reference.

As the image acquisition systems dedicated to small animals (like MicroCT and MicroMRI) have been improved and widespread, more anatomically realistic phantoms were built based on 3D images. Kolbert *et al.* (2003) presented a voxel phantom of female athymic mice constructed from a Magnetic Resonance Imaging – MRI

*Correspondence: B. M. Mendes. Centro de Desenvolvimento da Tecnologia Nuclear (CDTN/CNEN). Av. Antônio Carlos, 6627, Pampulha - 31270-901 Belo Horizonte, MG, Brazil. E-mail: bmm@cdtn.br or bmelom@yahoo.com.br

data set. In this study, only the kidney, liver, and spleen organs were segmented. Hindorf, Ljungberg, Strand (2004) published a new voxel phantom including more identified and segmented organs. Their masses were based on the mean values of ten dissected animals. It was an interesting approach from Hindorf's work. On the other hand, although it was a voxel phantom, the anatomy was not segmented from images. Thus, the organs and the animal itself were still defined as a set of simplified geometric shapes.

Segars *et al.* (2004) developed a 4D animal phantom called "Moby." The model was based on high-resolution MRI of a C57BL/6 male mouse. Non-uniform rational B-spline surfaces (NURBS) were applied in Moby construction. This has allowed the modeling of internal organs motion due to heartbeat and breathing. The model was applied later in several mice dosimetry studies (Bretin *et al.*, 2013; Taschereau, Chatziioannou, 2007; Larsson *et al.*, 2007; Boutaleb *et al.*, 2009; Keenan *et al.*, 2010; Larsson *et al.*, 2011; Mauxion *et al.*, 2013; Xie, Zaidi, 2013; Lin *et al.*, 2014).

Situ, Hoffman, Hartmann (2005) and Stabin *et al.* (2006) published voxel phantoms of mice with segmentation process based on MicroCT images. Bitar *et al.* (2007); Bitar, Lisboa, Bardiès (2007) implemented a mouse phantom of a female athymic "nude" strain. In this work, MicroCT or MicroMRI images were not used. The voxel model was constructed from high-resolution color images generated from 0.1 mm thickness coronal slices of the animal frozen body (Color Cryosections).

Stout *et al.* (2002) created and made available a set of co-registered images of MicroCT, PET, and Cryosections of a male nude mouse of 28 g (Stout *et al.*, 2002; Dogdas *et al.*, 2007). The project was called "Digimouse." Three voxel phantoms were produced from Digimouse data set: Boutaleb *et al.* (2009), Mohammadi, Kinase (2011a, b) and Zhang *et al.* (2012). Mohammadi, Kinase (2011a) presented Specific Absorbed Fractions (SAF) for diverse energies photons, using EGS4 Monte Carlo code. Several source and target organs were considered. These data allow validation studies of absorbed dose calculation protocols.

The aim of this study was to create a new voxel phantom from "Digimouse" project images to absorbed dose calculation for mice experiments conducted in our institutions. The model was prepared to run in MCNPx Monte Carlo code. The obtained phantom was called DM_BRA. The volume and mass of segmented organs were compared with those presented by Mohammadi, Kinase (2011a,b) and Zhang *et al.* (2012). Simulations were performed using MCNPx for exemplification. The heart was considered the source organ. Photons of diverse

energies were simulated, and SAF values obtained. The data were compared with those published by Mohammadi, Kinase (2011).

MATERIAL AND METHODS

Model construction

A set of Micro-CT images of Digimouse project, kindly provided, was chosen for the segmentation process (Stout *et al.*, 2002; Dogdas *et al.*, 2007). It represents a male mouse (*Mus musculus*) of nude strain, weighing 28 g. The images composed a matrix of 380x992x208 elements of 0.1 mm³ voxel size. Forty-two coronal slices, normal to the plane z, spaced by 0.5 mm, were manually segmented. Corel Photopaint® was used for selecting and assigning a specific color for each organ/tissue. The computer used for the segmentation process was a notebook with an Intel core i5® processor and 4 GB memory. The Atlas of Digimouse project was used to help perform the identification procedure.

ImageJ® software was applied to assemble the segmented images in a 3D stack. This software was also used to reduce the data set resolution from 380x992x208 to 152x396x42. The voxel dimensions resulting were 0.25x0.25x0.50 mm³. The set of images was converted to 8bits unassigned and saved in binary format (.raw).

A C++ program developed "in house" was used to read and convert the binary file to a voxel model template format readable on SISCODES software (Trindade, Campos, 2011). The SISCODES software was employed as an interface for generation of input files for running in MCNPx.

The tissue chemical compositions and densities (g/cm³) were based on human data, present in ICRP 110 (ICRP, 2009). The bone tissues were defined from values given in ICRU (1989).

Monte Carlo simulations

MCNPx (v. 2.7.0) Monte Carlo code was adopted on simulations (Pelowitz, 2011). It was installed on a 120 core cluster at Laboratório de Nêutrons of the Instituto de Radioproteção e Dosimetria-IRD/CNEN. Similar to Mohammadi, Kinase (2011a), 0.015, 0.1, 0.5, 1 and 4 MeV source photons were considered in the simulations. The emissions have a uniform distribution inside the heart. The source organ was also set as target organ.

The absorbed dose in each voxel was calculated with +F6. This tally returns the energy deposited per unit of mass (MeV/g). The average absorbed dose was also

requested for each target organ in the simulations. Values of specific absorbed fraction (SAF) for each target organ were calculated from the average absorbed dose. The obtained values were compared with reference values (RV) published by Mohammadi, Kinase (2011a). The number of particle histories simulated (NPS) by MCNPx was set sufficiently high to ensure that the relative errors were less than 5% in all organs.

3D view of absorbed dose and relative errors

The heart was set as source organ for 3D visualization of absorbed dose patterns and relative errors distribution. A C++ program was developed to extract each voxel absorbed dose and relative error from MCNPx output files. Binary files “.raw” suitable for Amide® software were generated. Two binary files were obtained for each simulation: one containing the 3D absorbed dose deposition pattern and another showing the relative errors distribution pattern. Each organ’s average absorbed dose and relative error were also evaluated from output files.

Statistic Evaluation

SAF values obtained through +F6 tally were

compared with the SAF values provided by Mohammadi, Kinase (2011a). Hypothesis tests were performed to determine whether the differences between the averages could be considered statistically significant. The relative errors were found to be 5% for Mohammadi, Kinase (2011a) values. The significance level adopted was 0.01.

RESULTS

The DM_BRA voxel model

In this DM_BRA version, each organ was segmented as a uniform region. The distinction between wall and content for intestine, stomach, heart and bladder segmentations was not taken into account. The kidneys were not sectioned into regions either (i.e. cortex, medulla, and pelvis). The DM_BRA bones were segmented as a single structure, called skeleton. No distinction between cortical and trabecular bone (spongiosa) was made.

Figure 1 shows coronal (A), sagittal (B) and transverse (C) slices of DM_BRA model. Amide® software was used to generate the images. The renderization of the model (Fig.1D) and the skeleton (Fig.1E) were also included. Specific colors were assigned for each segmented organ. Twenty-two organs/tissues were

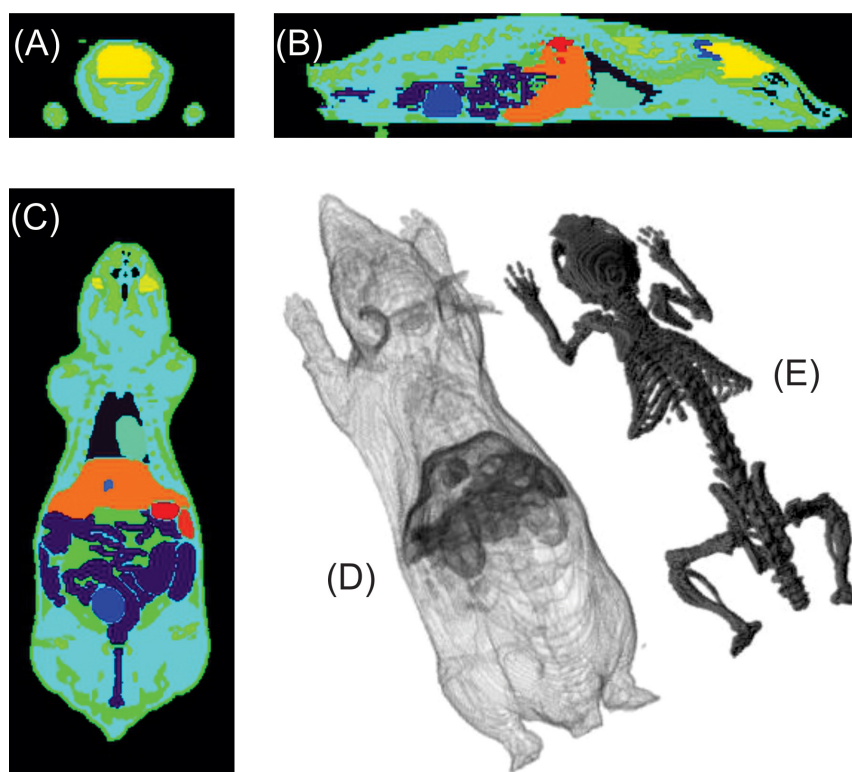


FIGURE 1 - Graphical representations of DM_BRA model obtained through the AMIDE® software. Coronal (A) Sagittal (B) and transversal (C) slices. Whole body (D) and skeleton (E) 3D rendering.

segmented: lung, intestine, eye, urinary bladder, brain, cerebellum, gall bladder, adrenal gland, Harderian glands, testis, muscle/soft tissue, adipose tissue, heart, spinal cord, skin, pancreas, bone, brown fat, kidney, liver, spleen, and stomach.

DM_BRA characteristics and data of main mice phantoms available in the literature are summarized in Table I, depicting the wide diversity of references elected by the researchers to set the chemical composition and density of the model's tissues. On the other hand, a

TABLE I - Summary of DM_BRA mouse voxel model characteristics and comparison with the main phantoms available in the literature

Study	Animal Weight (g)	Mouse Strain/sex	Voxel Dim. (mm ³)	Matrix	Segment. Data	Phantom type	Tissue Composition and Density
DM_BRA ^a	28	Nude/♂	0.25 x 0.25 x 0.50	152 x 396 x 42	CT/Cryos	voxel	ICRP (2009)
Xie, Zaidi (2013) ^a	21 - 35 ^d	C57BL/6/♂	0.20 x 0.20 x 0.20	200 x 200 x 512	MR	voxel	-
Mauxion <i>et al.</i> (2013) ^b	30	C57BL/6/♂	0.625 x 0.625 x 0.625 0.20 x 0.20 x 0.20	42 x 160 x 41 -	MR	voxel	Cristy, Eckerman, (1987)
Zhang <i>et al.</i> (2012) ^a	28	Nude/♂	0.20 x 0.20 x 0.20	190 x 496 x 100	CT/Cryos	voxel	ICRU (1991)
Larsson <i>et al.</i> (2011) ^b	22, 28, 34	C57BL/6/♂	0.22 x 0.22 x 0.22 0.23 x 0.23 x 0.23 0.25 x 0.25 x 0.25	160 x 160 x 432	MR	voxel	ICRP (1974)
Mohammadi, Kinase (2011b) ^a	28	Nude/♂	0.10 x 0.10 x 0.10 0.40 x 0.40 x 0.40	380 x 992 x 208 95 x 248 x 52	CT/Cryos	voxel	Cristy, Eckerman, (1987)
Keenan <i>et al.</i> (2010) ^b	25, 30, 35	C57BL/6/♂	0.625 x 0.625 x 0.625	-	MR	voxel	Cristy, Eckerman, (1987)
Boutaleb (2009) ^a	28	Nude/♂	0.2 x 0.2 x 0.2	190 x 496 x 104	CT/Cryos	voxel	ICRU (1989)
Taschereau, Chatziaoannou (2007) ^b	33	C57BL/6/♂	0.40 x 0.40 x 0.40	80 x 80 x 270	MR	voxel	ICRU (1991)
Larsson <i>et al.</i> (2007) ^b	33	C57BL/6/♂	0.25 x 0.25 x 0.25	128 x 128 x 432	MR	voxel	ICRP (1974)
Bitar <i>et al.</i> (2007)	30	Nude/♀	0.22 x 0.22 x 0.20	-	Cryos	voxel	ICRU (1989)
Stabin <i>et al.</i> (2006)	27	Transgenic/♂	0.20 x 0.20 x 0.20	256 x 256 x 256	CT	voxel	-
Segars <i>et al.</i> (2004) ^b	33	C57BL/6/♂	variable	Variable	MR	NURBS	-
Hindorf, Ljungberg, Strand (2004) ^c	24	-	0.39 x 0.39 x 0.39	64 x 64 x 166	-	voxel	Cristy, Eckerman, (1987)
Kolbert <i>et al.</i> (2003)	25	Nude/♀	0.10 x 0.10 x 0.12	256 x 256 x 256	MR	voxel	-
Yoriyaz, Stabin (1997)	-	-	-	-	-	stylized	-
Hui (1994) ^c	25	Nude/?	-	-	-	stylized	-

a- Based on digimouse (Stout *et al.*, 2002) data; b- Based on Moby Phantom (Segars *et al.*, 2004); c- Based on data of 10 animals; d- Seventeen models between 21g and 35g

low number of mice strains were represented as voxel models: C57BL/6 and Nude. A phantom of a transgenic mouse was also built, but the strain was not mentioned. Phantoms of mice weighing 21 g to 35 g were built. The smallest voxel dimension was (0.1x0.1x0.1) mm³ and the largest (0.625x0.625x0.625) mm³. DM_BRA model presented an intermediary (0.25x 0.25x0.50) mm³ voxel size.

Organ's masses for the DM_BRA model are shown in Table II. Other phantoms data from literature were also included. The voxel model total mass was 25.7g, a value 8% lower than expected since the animal originally weighed 28 g (Stout *et al.*, 2002). Wide variation among organ masses was seen in Table II. Urinary bladder, pancreas, spleen, and stomach had the highest ratios between maximum and minimum masses: 19.8, 10.7, 9.8

and 6.3 respectively. The organ mass ratio was higher than two for the majority of the organs.

The DM_BRA organ masses generally showed good agreement with those models generated from the same data set (Digimouse®). The analysis of the organs volumes is relevant to compare different segmentations since it eliminates the influence of different tissues density assigned by the various authors. Table III shows the organ volumes ratio for common organs of the three different Digimouse models. Also, the ratio between the maximum and minimum volume for each segmented organ was presented. Despite the fact that one of the mouse models of Boutaleb *et al.* (2009) work was based on Digimouse Atlas, it was not included in the comparison because the total mass of the model was scaled to 27 g and 33 g.

TABLE II - Organ and tissue masses segmented on DM_BRA and other voxel models available in literature

Organ/Tissue	Organ/Tissue mass (g) described in each study									
	DM_BRA ^a	Mohammadi, Kinase (2011a) ^a	Zhang <i>et al.</i> (2012) ^a	Boutaleb (2009) ^a	Taschereau, Chatziioannou (2007) ^b	Keenan <i>et al.</i> (2010) ^b	Mauxion <i>et al.</i> (2013) ^b	Bitar <i>et al.</i> (2007)	Hindorf, Ljungberg, Strand (2004) ^c	Stabin <i>et al.</i> (2006)
Adip. Tissue	2.379	-	-	-	-	-	-	1.859	-	-
Adrenals	0.005	0.006	0.004	-	-	-	-	0.011	-	-
Brain ^f	0.350	0.385	0.442	-	0.635	0.570	0.606	0.516	-	-
Brown Fat	0.142	-	-	-	-	-	-	-	-	-
Eye	0.006	0.006	0.004	-	-	-	-	-	-	-
Gall Bladder	0.009	-	-	-	-	-	-	-	-	-
Hard. Gland	0.032	0.032	-	-	-	-	-	-	-	-
Heart	0.215	0.232	0.218	0.264	0.120 ^e	0.290	0.283	0.282	0.120	0.143
Intestine	2.311	-	-	-	1.820	2.830	2.941	2.927	-	0.952
Kidney	0.482	0.515	0.478	0.586	0.415	0.370	0.379	0.377	0.280	0.334
Liver	1.987	2.087	2.010	2.373	2.690	2.150	2.177	1.831	0.890	0.780
Lung	0.167	0.124	0.096	0.121	0.130	0.110	0.098	0.123	0.150	0.125
Muscle/Soft	12.254	-	17.117	-	-	-	-	-	-	-
Pancreas	0.047	0.047	0.041	-	0.440	0.380	0.390	0.090	-	-
Skeleton	2.311	1.656	1.820	-	2.573	2.610	3.336	1.074	-	-
Skin	2.228	-	3.841	-	6.910	-	-	-	-	-
Spinal Cord	0.099	0.048	-	-	-	-	-	0.112	0.190	-
Spleen	0.140	0.144	0.132	0.164	0.130	0.140	0.137	0.216	0.090	0.022
Stomach	0.245	0.235	0.254	0.264	0.085 ^d	0.069 ^c	0.070 ^c	0.438	-	0.298
Testes	0.159	0.156	0.136	1.76	0.400	0.200	0.188	-	0.250	0.141
Thyroid	-	-	-	-	0.015	0.020	0.017	0.005	0.020	-
U. Bladder	0.238	0.197	0.205	-	0.045 ^d	0.080	0.078	0.025	0.060	0.012
Total Body	25.7	23.4	26.9	27.0	32.8	29.8	30.2	30.7	24.0	-

a- Based on digimouse data (Stout *et al.*, 2002); b- Based on Moby Phantom (Segars *et al.*, 2004); c- Based on data of 10 animals; d- Only the organ wall mass was available; e- Content filled with air; f- Cerebrum and Cerebellum

TABLE III - Ratio between organ volumes of organs common to Digimouse images based models. Maximum and minimum volumes ratios were also presented

Tissue/Organ	Organ volumes ratio			Ratio max/min Volume
	DM_BRA / Mohammadi, Kinase (2011a)	DM_BRA /Zhang <i>et al.</i> (2012)	Mohammadi, Kinase (2011a)/Zhang <i>et al.</i> (2012)	
Adrenals	0.838	1.255	1.499	1.499
Brain	0.900	0.784	0.872	1.275
Eye	0.997	1.496	1.501	1.501
Heart	0.919	0.996	1.084	1.084
Kidney	0.927	1.008	1.088	1.088
Liver	0.943	0.998	1.058	1.058
Lung	1.050	1.187	1.130	1.187
Pancreas	1.001	1.136	1.134	1.134
Skeleton	1.396	1.270	0.910	1.396
Spleen	0.970	1.082	1.115	1.115
Stomach	1.043	0.954	0.914	1.094
Testes	1.021	1.167	1.143	1.167
U. Bladder	1.204	1.152	0.956	1.204
Remaining Tissues	1.110	1.078	0.971	1.110

Table III demonstrates that eyes and adrenal (small organs) segmentation resulted in the largest volumes differences among the models (~50%). Large organs or tissues such as skeletal and brain also exhibited significant variations: 40% and 27% respectively. The other organs showed maximum/minimum volume differences equal or less than 20%.

Monte Carlo simulations

Table IV shows the SAF values calculated using DM_BRA model adapted to MCNPx code. The SAF graphics were included in Supplementary Information. The organs average absorbed doses were obtained through +F6 tally and then converted into SAF. Values obtained by Mohammadi, Kinase (2011a) were used as a reference.

The relative errors (RE) were kept below 5% for most organs in the simulations. Only the bladder and adrenal SAF errors were greater than 5% (but less than 20%). The small size of adrenals makes it difficult to obtain low relative errors when they are relatively far from source organ. The bladder, despite being a medium-sized organ, is one of the most distant organs from heart. Despite this, only cases with 15 keV photons showed RE greater than 5%. The total simulation time varied among

the cases. The shorter simulation time was approximately 8 hours for 15 keV photons, and the greater was about 18 hours for 4 MeV photons. The main reasons for the high computational times were the evaluation of the absorbed dose per voxel and electron transport setup (mode p e and + F6 tally).

Differences between MCNPx +F6 tally (Table IV) and Mohammadi, Kinase (2011a) SAF values were equal or less than 10% for most cases/organs. The discrepancies were not statistically significant for the heart, spleen, pancreas, liver, kidneys, and adrenals, considering all simulated cases. Skeleton presented highest deviations: 20% to 33% underestimations. Stomach SAF values, on the other hand, showed systematic overestimation. Lungs show differences statistically significant for low energy photons (0.015 keV and 0.1 keV). Urinary bladder's SAF values were statistically different only for 15keV photons.

The graphic of Specific Absorbed Fraction (SAF) versus energy of emitted photons in the mouse heart for some DM_BRA phantom organs can be seen in Figure 2. Note that a change in curve shape is observed as the distance between the source organ and the target organ increases, especially at low energy. The local minimum point at 100 keV does not exist for the bladder and testicles (the most distant organs).

TABLE IV - Specific Absorbed Fraction (SAF) for different organs calculated using MCNPx +F6 tally. Comparison with reference values published by Mohammadi, Kinase (2011a)

Photon Specific Absorbed Fractions - SAF (1/kg) – Source Organ = Heart											
Energy (MeV)	Study	Skeleton	Heart	Bladder	Stomach	Spleen	Pancreas	Liver	Kidneys	Adrenal	Lungs
0.015	Mohammadi, Kinase (2011a)	6.8E+01	1.2E+03	1.9E-01	8.4E+00	2.8E+00	2.5E+00	3.8E+01	1.6E+00	4.8E+00	2.7E+02
	DM_BRA	4.6E+01	1.3E+03	2.4E-01	1.1E+01	3.1E+00	2.9E+00	3.5E+01	1.5E+00	4.5E+00	3.1E+02
	Ratio	0.67*	1.10	1.24*	1.33*	1.11	1.17	0.91	0.95	0.93	1.14*
0.1	Mohammadi, Kinase (2011a)	1.7E+00	3.1E+01	2.3E-01	1.0E+00	6.1E-01	5.7E-01	2.0E+00	4.6E-01	7.8E-01	7.5E+00
	DM_BRA	1.3E+00	3.1E+01	2.3E-01	1.3E+00	6.4E-01	6.3E-01	2.0E+00	4.8E-01	6.4E-01	8.5E+00
	Ratio	0.76*	1.01	0.99	1.25*	1.05	1.10	0.98	1.03	0.82	1.14*
0.5	Mohammadi, Kinase (2011a)	1.5E+00	3.6E+01	2.9E-01	1.3E+00	7.3E-01	6.9E-01	2.5E+00	5.9E-01	9.7E-01	9.5E+00
	DM_BRA	1.1E+00	3.6E+01	2.9E-01	1.50E+00	8.1E-01	7.2E-01	2.4E+00	6.0E-01	9.8E-01	1.1E+01
	Ratio	0.75*	1.00	1.00	1.15*	1.11	1.04	0.95	1.02	1.01	1.11
1	Mohammadi, Kinase (2011a)	1.4E+00	2.7E+01	2.9E-01	1.2E+00	7.2E-01	6.7E-01	2.4E+00	5.6E-01	8.1E-01	8.3E+00
	DM_BRA	1.0E+00	2.6E+01	2.8E-01	1.4E+00	7.9E-01	7.3E-01	2.2E+00	5.8E-01	8.3E-01	9.2E+00
	Ratio	0.74*	0.96	0.95	1.17*	1.10	1.08	0.93	1.03	1.03	1.10
4	Mohammadi, Kinase (2011a)	5.3E-01	4.4E+00	1.8E-01	7.7E-01	4.9E-01	4.9E-01	1.0E+00	3.9E-01	6.2E-01	1.8E+00
	DM_BRA	4.3E-01	4.1E+00	1.9E-01	8.2E-01	5.1E-01	4.9E-01	9.8E-01	3.8E-01	6.8E-01	1.9E+00
	Ratio	0.80*	0.94	1.03	1.07	1.05	1.01	0.98	0.99	1.10	1.03

* - Difference between the means are statistically significant (Significance level = 0.01)

Spatial distributions of absorbed doses and relative errors

The absorbed dose values were normalized for the maximum value obtained in the simulation. Figure 3 shows coronal slices exported from Amide® software. NIH table was used to set colors to each voxel according to the normalized absorbed dose. An image of the model was fused to the absorbed dose image to improve the visualization and the organ localization.

Target organs located farther from the source, such as the bladder, showed relative errors per voxel up to 100%, for lower energy photons with +F6 tally as it was shown in Figure 3. When considering the total organ volume for absorbed dose sampling, relative errors were less than 5% for most organs, as previously mentioned.

Cases with 15 keV photons source showed that

higher absorbed dose values were observed in ribs and sternum inner surfaces (Figure 4). Skeleton average absorbed dose in these simulations were more than ten times lower than the heart, however, there are hot spots on thorax bones with highest absorbed doses. Figure 4 also shows that 100 keV photon deposited higher absorbed dose in rib cage bones than in the soft tissues near these bones. Energy deposition pattern was not influenced by bone tissues in simulations with 500 keV or greater energy photons. In these cases hard tissue near the heart shows the same behavior than their adjacent soft tissues.

DISCUSSION

This version of DM_BRA presents the segmentation of the organs as homogeneous tissues, with few internal details. Human phantom evolution shows that

segmentation in greater detail is a natural tendency with increasing computer processing power and memory.

Currently, ICRP reference phantoms (ICRP, 2009) present refined segmentation. Various organs show wall and content distinction at the ICRP phantoms. The assumption of segmentation of the distinct organ's wall and its content, as well as the kidney sectioning, will provide a model representation closer to the real animal than only considering the organ as a uniform mass. However, the magnitude of the differences in simulations when either approach is adopted was not demonstrated for mice yet. Future DM_BRA versions will incorporate distinctions between organ's wall and its content as well as the kidneys sectioning in the marrow, cortex, and pelvis. As an example, DM_BRA bones were segmented as a single structure called skeleton. Optimal Bone marrow dosimetry for mice appears to be still a challenge. The chemical composition and density of the main bones or bones sets, as well as red bone marrow (RBM), yellow bone marrow

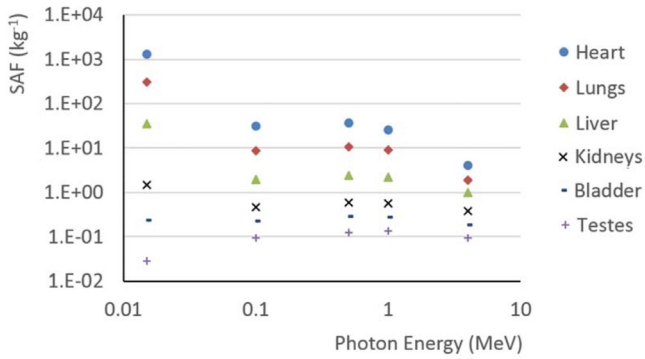


FIGURE 2 - Graphic of Specific Absorbed Fractions versus photon energy for some of DM_BRA organs. The photon source was positioned at the heart. The relative errors were below 5%.

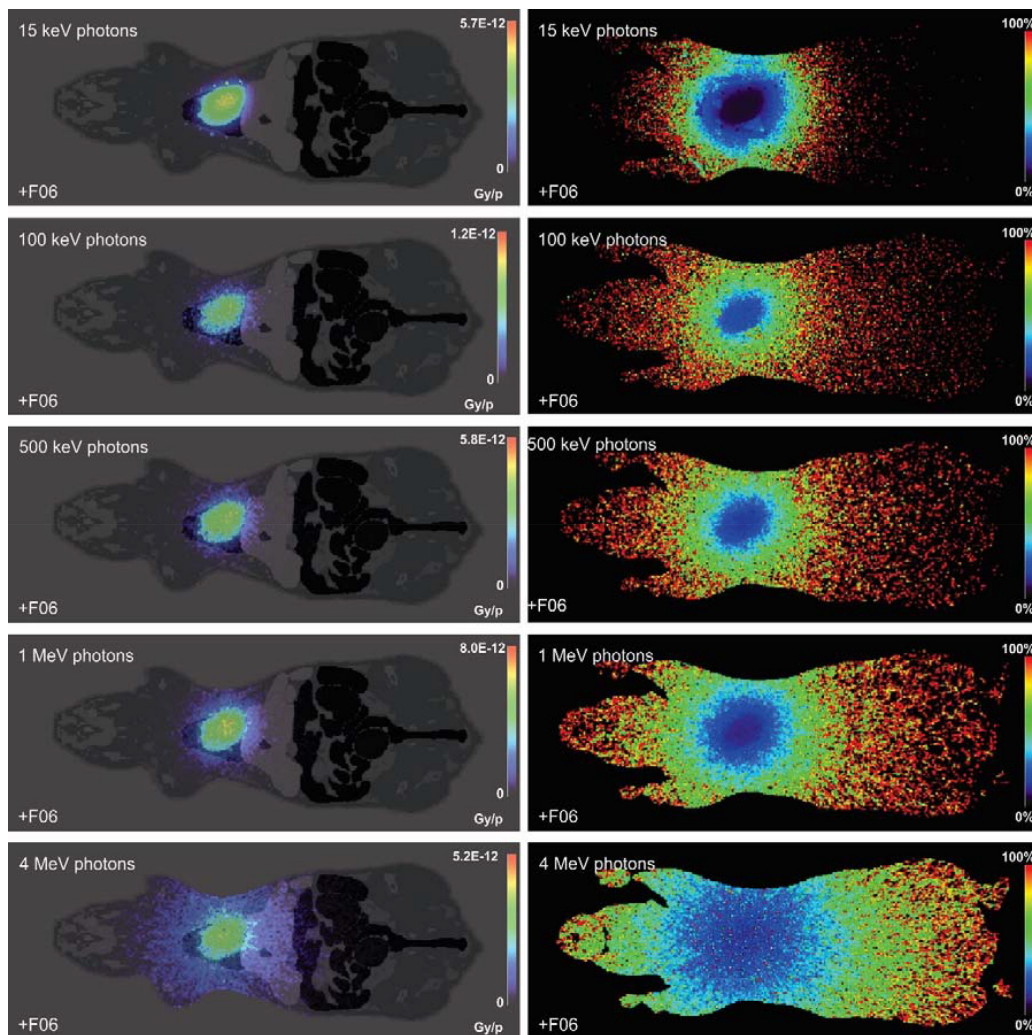


FIGURE 3 - Coronal slices from Amide® software presenting the absorbed doses (left side) and relative errors (right side) distribution pattern for 15 keV, 100 keV, 500 keV, 1 MeV or 4 MeV photon emitted at heart. The values were evaluated with +F6 tally. NPS was set to 1E+06.

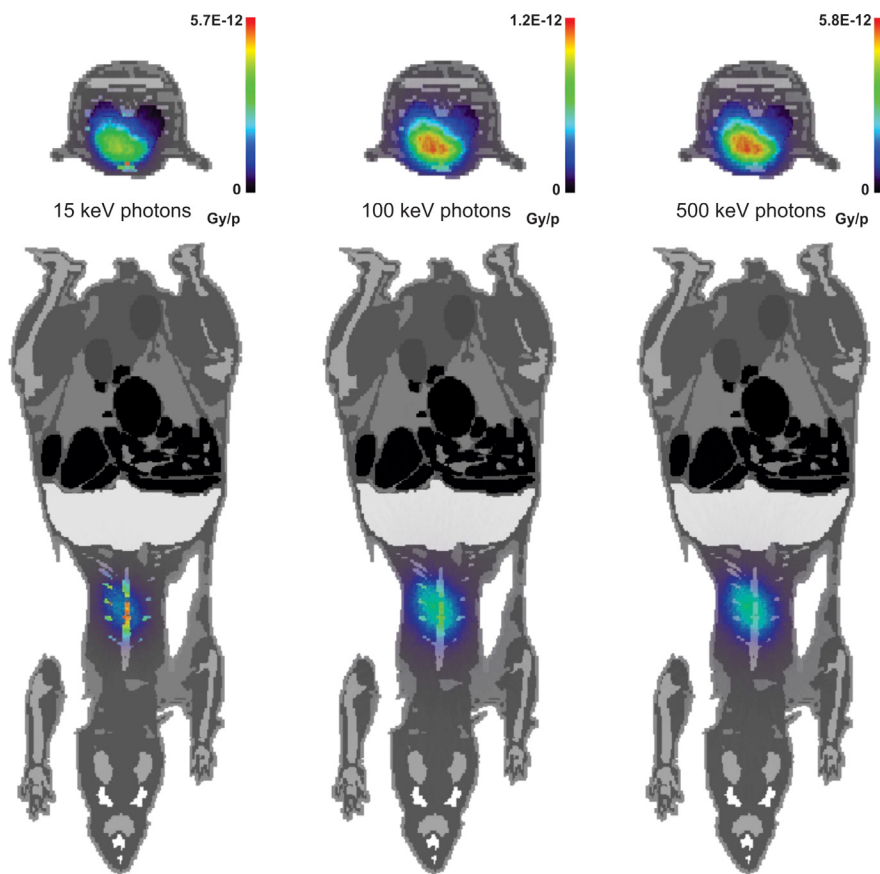


FIGURE 4 - Transversal and coronal slices of absorbed doses distribution pattern fused with model representation image. The maximum absorbed doses per emitted particle were spotted on ribs inner surfaces for a 15 keV photons at heart source. For 100 keV to 500 keV photons the maximum absorbed dose was observed in the heart.

(YBM) and mineralized bone (bone mineral) percentages were established for humans (ICRP, 2002). These data do not exist or are not easily accessible for mice. ICRP 110 human reference phantoms present distinctions between cortical and trabecular region (spongiosa). Long bones also show medullary cavity and are divided into proximal and distal regions (ICRP, 2009). For bone marrow absorbed dose evaluation, the simple transposition of human data and calculation methods to murine models does not seem adequate. These procedures will drive the future work on DM_BRA phantom.

The wide diversity of references to set the chemical composition and density of the model's tissues was observed in Table I. Such occurrence makes it difficult for the intercomparison's procedure. Furthermore, there is no easy method to identify the best data from references that should be adopted, while a more modern set of data from human reference is not necessarily closer to mice values. The generation of reference values for chemical composition, density, and mass of mice organs shall be a good contribution to small animal dosimetry. Also, DM_

BRA whole body mass (25.7 g) was 8% lower than the expected (28 g). Mohammadi, Kinase (2011b) and Zhang *et al.* (2012) also reported models with smaller masses than the real: 23.4 g and 26.9 g respectively. Segmentation errors can be a cause of the mass differences. Another explanation may be the adopted tissue density. Zhang *et al.* (2012) corroborates this statement. Chemical composition and density data from human organs have been adopted in these three studies. It is possible that such practice may generate errors on computational absorbed dose calculations. Mass of mouse models found in literature ranged from 21 to 35 grams. Much of the mice used in ionizing radiation experiments are within this weight. However, they were based only on segmentations of a few animals (Hindorf, Ljungberg, Strand, 2004; Kolbert *et al.*, 2003; Stabin *et al.*, 2006; Stout *et al.*, 2002; Bitar *et al.*, 2007; Segars *et al.*, 2004). Indeed, a large group of mouse models, including DM_BRA, were based on images of only two animals: the Digimouse project data (Nude-male) or phantom Moby (C57BL/6-male). Indeed, the existing mouse phantoms show low representativeness regarding

the morphological diversity of strains used in ionizing radiation experiments. Some important strains (BALB/c, SCID, Swiss, etc.) have not been segmented until now.

Table II shows a large difference between maximum and minimum organ masses. For most organs, it was higher than 100%. The following factors may have contributed to the observed discrepancies: i) organ condition at the image acquisition (e.g. bladder - full or empty); ii) differences in organ assigned material (e.g. stomach - filled with air in some cases); iii) different densities assigned to the same tissue (e.g. lung - 0.26 to 0.38 g/cm³); iv) distinct model voxels dimensions (especially affects small organs such as the thyroid and adrenal); v) subjectivity and errors during segmentation; and vi) the inherent variability of organ mass of different mice strains.

Tally +F6 SAF values agreed with Mohammadi, Kinase (2011a) results for most organs and photon energies. Main deviations were observed for the skeleton, stomach, and lungs. DM_BRA skeleton mass is 40% higher than Mohammadi, Kinase (2011a) model one. It is possible that this mass variation explains the SAF underestimations observed for this organ. The ratio between lung volumes of these models is only 1.05. Thus the adoption of different lung densities for the models should have led to DM_BRA SAF value overestimation. DM_BRA has a lung density of 0.382 g/cm³ while Mohammadi, Kinase (2011a) model adopted 0.296 g/cm³. That makes DM_BRA lung mass ~36% larger than Kinase's model. Stomach's mass presents little variation between the two models (4%). Possibly, differences in organ shape and distance from the source can explain deviations observed for this organ. On the other hand, adrenals and urinary bladder show substantial differences between the models referring to organ mass and volume. However, statistically significant differences were not observed in SAF values calculated for these organs. The exception is bladder's SAF for 15keV photons. The most important restriction to +F6 tally utilization was the high computational time required for calculations.

The 3D view of the absorbed dose deposition patterns complements the information addressed by the absorbed dose average at organs. We show in this work that 15 keV photons emitted on the heart produce hot spots of absorbed dose in ribs and sternum inner surfaces. Dosimetry restricted only to average absorbed doses evaluation does not allow the identification of particular situations as the one described. Relative error distribution visualization shows that even for small models, such as mice, the uncertainties grow very large for organs located far from the source. Since the target organ with the highest relative error determines the NPS needed to maintain

ER lower than the defined threshold. When the highest relative error organ reaches the acceptable error level (e.g. 5%), organs closer to the source generally have RE lower than 1%. Variance reduction methods can enhance errors distribution. Application of such techniques can greatly reduce the computational time maintaining the results reliability.

CONCLUSIONS

DM_BRA mouse voxel model was developed holding all suitable features of a mice phantom model. The SAF data in most simulated cases were statistically equal to those present in Mohammadi, Kinase (2011a), which provide a validation to the DM_BRA. The current configuration allows absorbed dose evaluations on multiple radioactive procedures involving radiopharmaceutical uses. The models created up to date are from a few mice image datasets. Thus, it exhibits low representativeness regarding mice morphological diversity. Studies should be conducted to determine intra-strain morphological variability. If low variability is observed for individuals with similar characteristics (age, sex, strain), the construction of specific reference mice phantoms could be justified (Mauxion *et al.*, 2013).

The visualization of absorbed dose spatial distribution brought improvements in the dosimetric analysis, complementing the information of the organ average absorbed dose. High absorbed dose spots in organs/tissues regions could be identified quantified and correlated with possible deterministic biological effects. Similarly, the depicting of relative errors per voxel can be useful in the evaluation of the variance reduction techniques effectiveness. In future studies, better patterns of errors distributions should be pursued.

ACKNOWLEDGMENTS

We would like to thank Dr. David Stout and Digimouse[®] project of the University of Southern California for having kindly provided the mouse images. We also thank the Laboratório de Metrologia de Nêutrons of the Instituto de Radioproteção e Dosimetria (IRD/CNEN) for consenting the use of high-performance cluster for the calculations. This research project is supported by the following Brazilian institutions: Departamento de Engenharia Nuclear (DEN) of Universidade Federal de Minas Gerais (UFMG), Centro de Desenvolvimento da Tecnologia Nuclear (CDTN), Comissão Nacional de Energia Nuclear (CNEN), Fundação de Amparo à Pesquisa de Minas Gerais (FAPEMIG – Projeto Universal), and

Conselho Nacional de Desenvolvimento Científico e Tecnológico (CNPq-REBRAT-SUS).

REFERENCES

- BOUTALEB, S.; POUGET, J.-P.; HINDORF, C.; PÈLEGRIN, A.; BARBET, J.; KOTZKI, P.-O.; BARDIÈS, M. Impact of mouse model on preclinical dosimetry in targeted radionuclide therapy. *Proc. IEEE*, v.97, p.2076-2085, 2009.
- BITAR, A.; LISBONA, A.; THEDREZ, P.; SAI MAUREL, C.; LE FORESTIER, D.; BARBET, J.; BARDIÈS, M. A voxel-based mouse for internal dose calculations using Monte Carlo simulations (MCNP). *Phys. Med. Biol.*, v.52, p.1013-1025, 2007.
- BITAR, A.; LISBONA, A.; BARDIÈS, M. S-factor calculations for mouse models using Monte-Carlo simulations. *Q. J. Nucl. Med. Mol. Imaging*, v.51, n.4, p.343-351, 2007.
- BRETIN, F.; MAUXION, T.; BAHRI, M.A.; LUXEN, A.; PLENEVAUX, A.; BARDIÈS, M.; SERET, A. *Absorbed doses to mice for three [¹⁸F]-tracers calculated from experimental kinetic data and Monte Carlo simulations*. 2013. Available from: http://orbi.ulg.ac.be/bitstream/2268/156160/1/EANM13_PosterAbstract.pdf. Access on: Aug. 18, 2015.
- CARLSON, S.K.; CLASSIC, K.L.; BENDER, C.E.; RUSSEL, S.J. Small animal absorbed radiation dose from serial micro-computed tomography imaging. *Mol. Imaging Biol.*, v.9, p.78-82, 2007.
- CRISTY, M.; ECKERMAN, K.F. *Specific absorbed fractions of energy at various ages from internal photon sources. I. Methods*. Oak Ridge: Oak Ridge National Laboratory, 1987. 100 p.
- DOGDAS, B.; STOUT, D.; CHATZHOANNOU, A.; LEAHY, R.M. Digimouse: A 3D whole body mouse atlas from CT and cryosection data. *Phys. Med. Biol.*, v.52, p.577-587, 2007.
- FLYNN, A.A.; GREEN, A.J.; PEDLEY, R.B.; BOXER, G.M.; BODEN, R.; BEGENT, R.H.J. A mouse model for calculating the absorbed beta-particle dose from ¹³¹I- and ⁹⁰Y-labeled immunoconjugates, including a method for dealing with heterogeneity in kidney and tumor. *Radiat. Res.*, v.156, p.28-35, 2001.
- HINDORF, C.; LJUNGBERG, M.; STRAND, S.E. Evaluation of parameters influencing S values in mouse dosimetry. *J. Nucl. Med.*, v.45, p.1960-1965, 2004.
- HUI, T.E.; FISHER, D.R.; KUHN, J.A.; WILLIAMS, L.E.; NOURIGAT, C.; HUTCHINSON, F.; BADGER, C.C. A mouse model for calculating cross-organ beta doses from yttrium-90-labeled immunoconjugates. *Cancer*, v.73, n.3, suppl., p.951-957, 1994.
- INTERNATIONAL COMMISSION ON RADIOLOGICAL PROTECTION. ICRP. *Report of the task group on reference man*. Oxford: Pergamon Press, 1974. (ICRP Publication, 23).
- INTERNATIONAL COMMISSION ON RADIOLOGICAL PROTECTION. ICRP. *Basic anatomical and physiological data for use in radiological protection: reference values*. Oxford: Pergamon Press, 2002. (ICRP Publication, 89).
- INTERNATIONAL COMMISSION ON RADIOLOGICAL PROTECTION. ICRP. *Adult reference computational phantoms*. Oxford: Pergamon Press, 2009. (ICRP Publication, 110).
- INTERNATIONAL COMMISSION ON RADIATION UNITS & MEASUREMENTS. ICRU. *Tissue substitutes in radiation dosimetry and measurement (Report 44)*. Bethesda: International Commission on Radiation Units & Measurements, 1989.
- INTERNATIONAL COMMISSION ON RADIATION UNITS & MEASUREMENTS. ICRU. *Photon, electron, proton, and neutron interaction data for body tissues (Report 46)*. Bethesda: International Commission on Radiation Units & Measurements, 1991.
- KEENAN, M.A.; STABIN, M.G.; SEGARS, W.P.; FERNALD, M.J. RADAR realistic animal model series for dose assessment. *J. Nucl. Med.*, v.51, n.3, p.471-476, 2010.
- KOLBERT, K.S.; WATSON, T.; MATEI, C.; XU, S.; KOUTCHER, J.A.; SGOUROS, G. Murine S factors for liver, spleen, and kidney. *J. Nucl. Med.*, v.44, n.5, p.784-791, 2003.
- LARSSON, E.; LJUNGBERG, M.; STRAND, S.E.; JÖNSSON, B.A. Monte Carlo calculations of absorbed doses in tumors using a modified MOBY mouse phantom for pre-clinical dosimetry studies. *Acta Oncol.*, v.50, n.6, p.973-980, 2011.

- LARSSON, E.; STRAND, S.E.; LJUNGBERG, M.; JÖNSSON, B.A. Mouse S-factors based on Monte Carlo simulations in the anatomical realistic moby phantom for internal dosimetry. *Cancer Biother. Radio*, v.22, n.3, p.38-442, 2007.
- LIN, H.H.; CHUANG, K.S.; LIN, Y.H.; NI, Y.C.; WU, J.; JAN, M.L. Efficient simulation of voxelized phantom in GATE with embedded SimSET multiple photon history generator. *Phys. Med. Biol.*, v.59, p.6231-6250, 2014.
- MAUXION, T.; BARBET, J.; SUHARD, J.; POUGET, J.P.; POIROT, M.; BARDIÈS, M. Improved realism of hybrid mouse models may not be sufficient to generate reference dosimetric data. *Med. Phys.*, v.40, n.5, p.1-13, 2013.
- MOHAMMADI, A.; KINASE, S. Monte Carlo simulations of photon specific absorbed fractions in a mouse voxel phantom. *Prog. Nucl. Sci. Technol.*, v.1, p.126-129, 2011a.
- MOHAMMADI, A.; KINASE, S. Influence of voxel size on specific absorbed fractions and S-values in a mouse voxel phantom. *Radiat. Prot. Dosim.*, v.143, n.2/4, p.258-263, 2011b.
- PELOWITZ, D.B. *MCNPx user's manual*. Version 2.7.0. Los Alamos, USA, 2011. p.645.
- PETOUSSI-HENSS, N.; ZANKL, M. Voxel anthropomorphic models as a tool for internal dosimetry. *Radiat. Prot. Dosim.*, v.79, n.1/4, p.415-418, 1998.
- SEGARS, W.P.; TSUI, B.M.W.; FREY, E.C.; JOHNSON, G.A.; BERR, S.S. Development of a 4D digital mouse phantom for molecular imaging research. *Mol. Imaging Biol.*, v.6, p.149-159, 2004.
- SITU, P.D.; HOFFMAN, T.J.; HARTMANN, S.C.L. Voxel based absorbed fractions in mouse digestive organs for therapeutic beta emitters. *J. Nucl. Med.*, v.46, n.2, Suppl., p.2278, 2005.
- SNYDER, W.S.; FORD, M.R.; WARNER, G.G. *Estimates of specific absorbed fractions for photons sources uniformly distributed in various organs of a heterogeneous phantom*. Oak Ridge: Ridge National Laboratory, 1978. 67p. (MIRD Pamphlet n.5). Revised). Available from: <http://interactive.snm.org/docs/MIRD%20Pamphlet%205.pdf>. Access on: Jan. 20, 2016.
- STABIN, M.G.; PETERSON, T.E.; HOLBURN, G.E.; EMMONS, M.A. Voxel-based mouse and rat models for internal dose calculations. *J. Nucl. Med.*, v.47, n.4, p.655-659, 2006.
- STOUT, D.; CHOW, P.; SILVERMAN, R.; LEAHY, R.M.; LEWIS, X.; GAMBHIR, S.; CHATZIOANNOU, A. Creating a whole body digital mouse atlas with PET, CT and cryosection images. *Mol. Imaging Biol.*, v.4, n.4, p.S27, 2002.
- TASCHEREAU, R.; CHATZIOANNOU, A.F. Monte Carlo simulations of absorbed dose in a mouse phantom from 18-fluorine compounds. *Med. Phys.*, v.34, n.3, p.1026-1036, 2007.
- TRINDADE, B.M.; CAMPOS, T.P.R. Sistema computacional para dosimetria de nêutrons e fótons baseado em métodos estocásticos aplicado a radioterapia e radiologia. *Radiol. Braz.*, v.44, n.2, p.109-116, 2011.
- WANG, G.J.; CAI, L. Induction of cell-proliferation hormesis and cell-survival adaptive response in mouse hematopoietic cells by whole-body low-dose radiation. *Toxicol. Sci.*, v.53, p.369-376, 2000.
- XIE, T.; ZAIDI, H. Monte Carlo-based evaluation of S-values in mouse models for positron-emitting radionuclides. *Phys. Med. Biol.*, v.58, p.169-182, 2013.
- XU, G.X.; ECKERMAN, K.F. *Handbook of anatomical models for radiation dosimetry*. Boca Raton: CRC Press, 2009. 757p.
- YONEZAWA, M. Induction of radio-resistance by low dose X-irradiation. *Yakugaku Zasshi*, v.126, n.10, p.833-840, 2006.
- YORIYAZ, H.; STABIN, M. Electron and photon transport in a model of a 30 g mouse. *J. Nucl. Med.*, v.38, Suppl., p.228, 1997.
- ZHANG, X; XIE, X; CHENG, J; NING, J; YUAN, Y; PAN, J; YANG, G. Organ dose conversion coefficients based on a voxel mouse model and MCNP code for external photon irradiation. *Radiat. Prot. Dosim.*, v.148, n.1, p.9-19, 2012.

Received for publication on 13rd May 2016
Accepted for publication on 11st October 2016